

RESEARCH

Open Access



# Influence of Initial Damage Degree on the Degradation of Concrete Under Sulfate Attack and Wetting–Drying Cycles

Yujing Lv<sup>1</sup>, Wenhua Zhang<sup>1\*</sup> , Fan Wu<sup>1</sup>, Huang Li<sup>1</sup>, Yunsheng Zhang<sup>2</sup> and Guodong Xu<sup>3</sup>

## Abstract

The previous researches on the degradation process of concrete under sulfate attack mainly focus on non-damaged concrete. It may lead to an excessive evaluation of the durability of the structure, which is detrimental to the safety of the structure. In this paper, three different damage degrees of concrete specimens with non-damaged ( $D_0$ ) and initial damage of 10% ( $D_1$ ) and 20% ( $D_2$ ) were prefabricated and subjected to sulfate attack and wetting–drying cycles. With the increase of sulfate attack cycles (0, 30, 60, 90, 120, 150 cycles), the changes in mass loss, relative dynamic modulus of elasticity, and the stress–strain curve were studied. The results show that the mass of the  $D_0$  specimen had been increasing continuously before 150 sulfate attack cycles. The mass of  $D_1$  and  $D_2$  had been increasing before 60 cycles, and decreasing after 60 cycles. At 150 cycles, the mass loss of  $D_0$ ,  $D_1$ ,  $D_2$  were  $-1.054\%$ ,  $0.29\%$  and  $3.20\%$ , respectively. The relative dynamic modulus of elasticity (RDME) of  $D_0$  specimen increases continuously before 90 sulfate attack cycles. After 90 cycles, the RDME gradually decreases. However, for  $D_1$  and  $D_2$  specimens, the RDME began to decrease after 30 cycles. The damage degree has an obvious influence on the compressive strength and elastic modulus. For the  $D_0$  specimen, the compressive strength and elastic modulus increased continuously before 90 cycles and decreased after 90 cycles. The compressive strength and elastic modulus of  $D_1$  and  $D_2$  specimens began to decrease after 30 cycles. The stress–strain curves of concrete with different initial damage degrees were established, and the fitting results were good. Finally, based on the analysis of experimental data, the degradation mechanism of concrete with initial damage under the sulfate wetting–drying cycle was discussed.

**Keywords:** initial damage, sulfate attack, wetting–drying cycles, mass loss, relative dynamic modulus, compressive strength

## 1 Introduction

Concrete is the most important building material in the world, widely used in coastal engineering and inland saline areas (Sun et al. 2013; Idiart et al. 2011). These areas are rich in sulfate ions and the sulfate attack is one of the most serious environmental damages. The sulfate attack affects the durability of concrete structures and causes huge economic losses. In recent years, much

research has been done on the mechanical properties (Aye and Oguchi 2011; Zuo and Sun 2009) and failure mechanism (Feng et al. 2015; Idiart et al. 2011) of concrete under sulfate attack environment.

Existing studies have shown that sulfate ions have corrosive effects and lead to degradation of concrete durability (Gao et al. 2013; Thaulow and Sahu 2004); (Helson et al. 2018) studied the durability potential of different soil–cement mixtures, and defined the critical thresholds relative to clay and cement content. They found that mechanical damage was the result of microcracking and ettringite expansion. Rozier et al. (2009) found that leaching and external sulfate attack of concrete would lead to

\*Correspondence: zhangwenhua2009@163.com

<sup>1</sup> School of Civil Engineering, Nanjing Forestry University, Nanjing 210037, China

Full list of author information is available at the end of the article  
Journal information: ISSN 1976-0485 / eISSN 2234-1315

the dissolution of hydration products. Expansion products would be formed when sulfate ions invaded. Not only the mass and morphology of concrete under leaching and external sulfate attack were analyzed, but also some microscopic pictures of crack growth were shown. It was found that the ettringite filled in the pores of the concrete, the pore structure of concrete, was changed. Jiang et al. (2016) prepared three different sulfate solutions and found that gypsum content in concrete corrosion products was lower than ettringite, and different types of sulfate solutions had a great impact on the number of corrosion products containing ettringite and gypsum. Chen et al. (2016) detected the damage evolution of concrete by the degradation of concrete modulus in a sulfate solution. The mechanism of microcrack formation was analyzed by Scanning Electron Microscope (SEM), and the differential equation of concrete internal expansion stress was derived. Those above researches mainly focused on the degradation of non-damaged concrete under sulfate attack.

However, in actual engineering, concrete structures often suffer damage due to inadequate casting and maintenance, premature loading, or accidental loading. These damages and cracks may accelerate the degradation speed of concrete structures under sulfate attack. Liu et al. (2020) investigated the mechanism of external sulfate attack on concrete under flexural fatigue loading and drying–wetting cycles. They found that fatigue loading causes cracking in the interfaces of various phases and forms cracks in the concrete. And the results showed that the fatigue loading and drying–wetting cycles can accelerate the transportation of sulfate ion inside the concrete and the deterioration degree of concrete subjected to sulfate. Chen et al. (2017) investigated the mechanism of the damage progress of concrete subject to combined sulfate–chloride attack under drying–wetting cycles and flexural loading. They found that flexural loading accelerates the deterioration of concrete subject to sulfate and chloride attack under dry–wetting cycles. Niu et al. (2015) investigated the failure mechanism of shotcrete under the combined actions of sulfate attack and drying–wetting cycles. Because of inherent inhomogeneity of shotcrete, the connected and loose defects could accelerate the intrusion of external sulfate ions and the growth of corrosion products. Zhou et al. (2018) prepared concrete specimens with a single crack, and observed the deterioration of corrosion samples near the crack tip by SEM. They found that with the increase of corrosion time, the corrosion depth near the crack tip of concrete gradually increased, and finally the concrete microstructure was porous and microcracks appeared. However, Zhou's research only targeted a single crack. In reality, there is a large number of micro-cracks in concrete (Siad et al. 2013; Bonakdar et al. 2012). At present, the service life prediction

of the concrete structure is based on the hypothesis of non-damage concrete, which may overestimate the durability and reliability of concrete structures. Therefore, it is necessary to study the degradation mechanism and mechanical properties of concrete with initial damage under sulfate attack.

In this paper, three different damage degrees of concrete specimens with non-damaged ( $D_0$ ) and initial damage of 10% ( $D_1$ ) and 20% ( $D_2$ ) were prefabricated and subjected to sulfate attack and wetting–drying cycles. The failure mode, mass loss, compressive strength, and relative dynamic elastic modulus of concrete with different initial damage degrees were measured and analyzed. The stress–strain model of concrete was established. Finally, the influence of the initial damage degree on the degradation mechanism of concrete under the sulfate attack and wetting–drying cycles was discussed.

## 2 Materials and Methods

### 2.1 Materials and Mixture Proportion

Concrete specimens, which had the compressive strength of 47.6 MPa at 28 days, were cast according to a mix proportion shown in Table 1. Chinese standard Graded P. I 42.5 Portland cement was used in the concrete specimens, produced by China Jiangnan Cement Co., LTD., with the specific surface area of 385 m<sup>2</sup>/kg. Table 2 offers its chemical composition. The coarse aggregate was of the continuous particle size of 5–20 mm. River sand, as fine aggregate, was 1.6 in fineness modulus.

The specimens were prepared as follows. First, cement, coarse aggregate, and fine aggregate were mixed and stirred for 1 min. When that mixture was mixed well it was swirled continuously for 3 min after being added water. Then, the mixed concrete slurry was poured into molds and vibrated at least for 15 s through a shaking table. Last, specimens were demolded when they were cured for 24 h at room temperature and were cured in standard curing room (20 °C, Relative Humidity (RH) 95%) for 28 days continuously.

### 2.2 Preparation of Initial Damage on Specimens

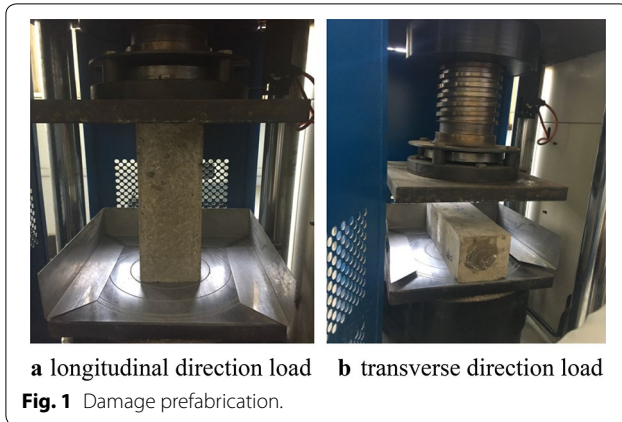
Before studying the influence of initial damage on the degradation of concrete under sulfate attack, it is necessary to prefabricate the concrete specimen with different damage degrees. The prefabrication process was carried out as the following.

**Table 1** Mix Proportion of concrete (kg/m<sup>3</sup>).

W/C	Cement	Water	Sand	Coarse aggregate
0.5	335	195	651	1157

**Table 2 Physical properties and chemical composition of cement.**

Physical properties		Chemical composition (%)							
Density (kg/m <sup>3</sup> )	Specific surface area (m <sup>2</sup> /kg)	CaO	SiO <sub>2</sub>	Al <sub>2</sub> O <sub>3</sub>	Fe <sub>2</sub> O <sub>3</sub>	SO <sub>3</sub>	K <sub>2</sub> O	Na <sub>2</sub> O	LOI
3150	369.6	62.6	21.35	4.67	3.31	2.25	0.54	0.21	0.95



- (1) First, three prismatic specimens were selected to carry out the uniaxial compression failure test. The ultimate compressive strength of the three specimens was measured and the average value was taken as the axial compressive strength of the specimens.
- (2) The initial wave velocity  $v_0$  in the longitudinal direction of a specimen was measured by the ultrasonic device before loading. A commercial UPV measurement device (Proceq) with two ultrasonic transducers was used to measure the P wave velocity. The transducers were of longitudinal wave type with a center frequency of 54 kHz and a diameter of 50 mm.
- (3) The stress of 60% of the axial compressive strength of the concrete was applied to the specimens at the longitudinal direction and transverse direction kept for 1 min, just as shown in Fig. 1. After loading each time, the P wave velocity  $v_t$  in the longitudinal direction of the specimen was measured, and the damage degree  $D_n$  of the concrete specimen is calculated by Eq. (1).

$$D_n = 1 - \frac{v_t^2}{v_0^2} \quad (1)$$

where  $D_n$  is the initial damage degree of the specimen,  $v_0$ (m/s) the ultrasonic velocity of the unloaded

specimen and  $v_t$  (m/s) the ultrasonic velocity of the specimen after loading.

- (4) There were three different damage degrees in this experiment: no initial damage  $D_0$  (damage degree is 0),  $D_1$  (damage degree is 0.1), and  $D_2$  (damage degree is 0.2), the error of damage degree was  $\pm 0.02$ . The initial damage degree of the specimen was prefabricated by controlling the loading times. Repeated loading on specimens was needed until the damage degree reached the predetermined value. The number of repeated loading in longitudinal and transverse directions was about 40 times for the specimen with a damage degree of 0.2.

### 2.3 Scheme of Sulfate Attack Test

A sulfate attack test can be carried out after the damage prefabrication of concrete specimens. The automatic sulfate drying–wetting cycle test machine was used. The test program was conducted as follows, which conforms to the requirements of GB/T 50082-2009 (GB 2009) in China.

First, the concrete specimens were immersed in  $Na_2SO_4$  solution with a mass fraction of 5% for 15 h. Second, the sulfate solution was drained and the concrete specimens were air-dried at room temperature for 1 h. Third, the concrete specimens were dried at 80 °C for 6 h. Finally, the specimens were cooled at room temperature for 2 h to room temperature. The duration of a sulfate attack drying–wetting cycle was 24 h. When the number of drying–wetting cycles reached 0, 30, 60, 90, 120, and 150 times, the specimens were taken out from the automatic sulfate drying–wetting cycle test machine. The surface of the specimen was wiped with a towel. Then, the mass  $m_n$  and ultrasonic pulse velocity  $v_n$  of the specimens with different initial damage degrees were measured immediately. This process can keep the specimen in the condition of saturated-surface-dry, which eliminates the influence of different moisture content on the ultrasonic wave speed and ensure the accuracy of each test result. According to the GB/T 50082-2009 (GB 2009) method, the mass loss of concrete specimen can be calculated by Eq. (2).

$$M_n = \frac{m_0 - m_n}{m_0} \quad (2)$$

where  $M_n$  is the mass loss of concrete specimen after  $n$  cycles of sulfate attack (%),  $m_0$  the average mass of concrete specimens before the sulfate attack (kg), and  $m_n$  the average mass of concrete specimens after  $n$  cycles of sulfate attack (kg).

Relative dynamic modulus of elasticity (RDME) can be calculated by Eq. (3) (Hu and Wu 2019; Wang et al. 2019)

$$E_{rd} = \left( \frac{v_n}{v_0} \right)^2 \quad (3)$$

where  $E_{rd}$  is the RDME of the concrete specimen after  $n$  cycles of sulfate attack,  $v_0$  the average ultrasonic pulse velocity of concrete before the sulfate attack (m/s), and  $v_n$  the average ultrasonic pulse velocity of concrete specimens after  $n$  cycles of sulfate attack (m/s).

#### 2.4 Uniaxial Compression Tests

Uniaxial compression tests were carried out on concrete specimens after different cycles of sulfate attack. The specimens were prism with a size of 100 mm × 100 mm × 300 mm. The electro-hydraulic servo pressure testing machine was used, just as shown in Fig. 2. For collecting the strain data, two displacement sensor LVDTs were arranged on each side of the clamps. All the experimental data were collected automatically by the TDS-530 Data Acquisition Instrument. A displacement-control procedure was applied during the axial compression test. To obtain continuous and steady curves, a slow displacement rate, 0.05 mm/min, was employed.



**Fig. 2** Setup for uniaxial compression test.

### 3 Test Results and Discussion

#### 3.1 Surface Characteristics of Sulfate-Attacked Concrete

Figure 3 presents the appearance of concrete with different initial damage degrees in different sulfate attack periods. It could be observed that with the increase of the sulfate drying–wetting cycles, the surface damage of concrete with the same initial damage was intensified. Taking the  $D_1$  specimen as an example, the surface of the specimen was light gray before the sulfate attack. After 60 days, a few micro-pores were formed on the surface of the specimen, but no obvious damage was found. After 90 days, a small number of ettringite and gypsum appeared on the surface of the specimen. After 150 days, the surface color of the specimen changed to dark brown, a large number of white crystals appeared on the surface of the specimen, and the edge of the specimen fell off. This is consistent with the phenomenon obtained by Zhou et al. (2018) through experiments.

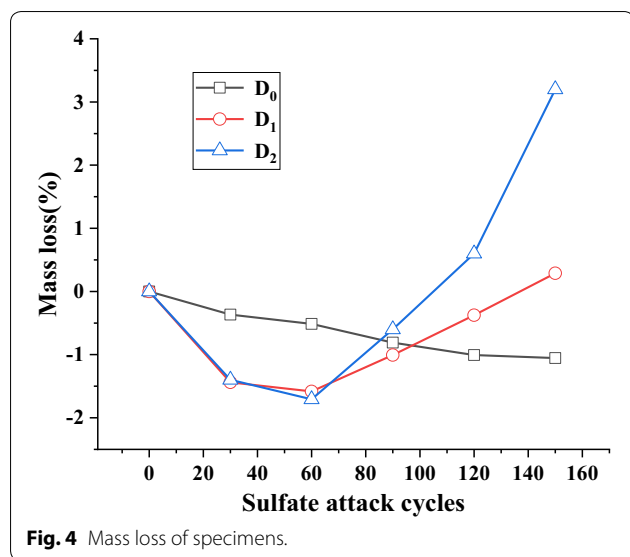
Besides, the initial damage degree has an important effect on the damage process of the specimen. The greater the initial damage was, the more serious the damage during the same sulfate attack period. As shown in Fig. 3, for  $D_0$ , when the sulfate attack days were 60 days, the change of the specimen was not obvious. After 150 days of the sulfate dry–wet cycle, the surface color of the  $D_0$  specimen turned brown. Except for a few pores, the appearance of the specimen was relatively complete, and there was no great change compared with before sulfate attack (Feng et al. 2015). However, compared with  $D_0$  specimens,  $D_1$  specimens and  $D_2$  specimens were damaged. After 60 days of sulfate dry–wet cycle, the edges of  $D_1$  prismatic specimens were damaged, while  $D_2$  specimens had peeling edges after 60 days of sulfate dry–wet cycle. After 150 days,  $D_1$  and  $D_2$  specimens were seriously damaged. The mortar on the surface of  $D_1$  specimens has completely fallen off, and aggregate exposed. The damage of  $D_2$  specimens was more serious, the surface layer was seriously peeling, edges and corners were missing, and cracks of large width appeared.

#### 3.2 Mass Change

Figure 4 shows the mass loss of specimens with different degrees of damage after the sulfate attack cycle. It can be found that the initial damage degree of concrete specimen has a significant impact on mass loss.  $D_1$  and  $D_2$  with initial damage show completely different characteristics from  $D_0$  without damage. For  $D_0$ , all mass loss values are negative in 150 cycles of sulfate attack, and with the increase of sulfate attack cycles, the mass loss curve shows a linear decrease. The data on the curve show that the mass of the  $D_0$  specimen has been increasing continuously. This means that the sulfate ions from outside



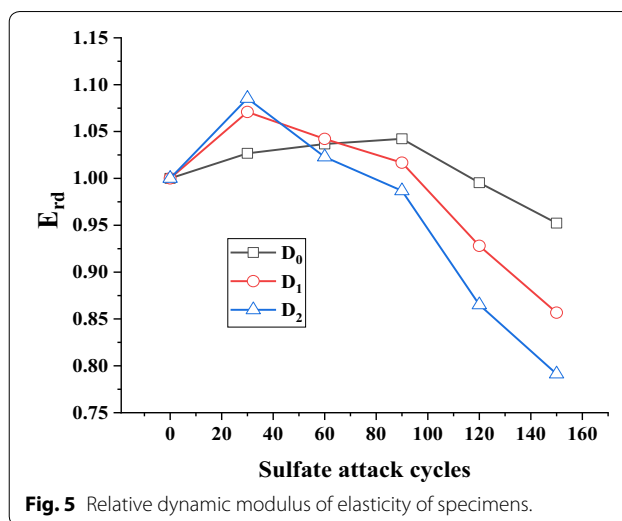
**Fig. 3** Surface characteristics of sulfate attacked concrete.



continuously permeate into the concrete and generate expansion products containing ettringite and gypsum (Sun et al. 2018), which leads to the continuous increase of the mass of concrete. At the same time, it also shows that the surface of the specimen has not been damaged, the mortar and aggregate have not been separated from the specimen, and the mass has not been lost. This experimental phenomenon is similar to the results of Hussein et al. (2018).

For  $D_1$  and  $D_2$  specimens with initial damage, the trend is different from that of  $D_0$ . In 60 cycles of sulfate attack, the curve value of the mass loss is negative and decreases with the increase of times. This indicates that the mass of  $D_1$  and  $D_2$  specimens is continuously increasing during this period. However, when the number of sulfate attack is more than 60 times, although the mass loss value is still negative, the direction of the mass loss curve has changed from the original downward to upward. Compared with the mass of 60 sulfate attack cycles, the mass of  $D_1$  and  $D_2$  specimens is reduced. The specimens have peeled off, resulting in mass loss.  $D_2$  with 20% damage showed a faster mass loss than  $D_1$  with 10% damage after 60 cycles. At 120 cycles, the mass loss of  $D_1$  was  $-0.375\%$ , but  $D_2$  was  $0.6\%$ . At 150 cycles,  $D_0$ ,  $D_1$  and  $D_2$  were  $-1.054\%$ ,  $0.29\%$  and  $3.20\%$ , respectively.

The mass change of concrete specimens during sulfate attack is mainly caused by the following reasons. First, in the early stage of sulfate attack, sulfate solution permeates into the concrete and fills the pores and cracks. Then, the sulfate ions interact with cement hydration products to form expansive products (ettringite, gypsum) to fill the pores and cracks, leading to an increase in the specimen mass (Irassar et al. 2003). As the sulfate attack



continues, the concrete internal damage became more and more serious as the products accumulated. This leads to mortar peeling and mass reduction of the concrete specimen. When the mass loss of concrete is greater than the sulfate solution entering the interior, the overall mass of the specimens decreases, and the mass loss increases.

For  $D_0$  specimens, 150 cycles of sulfate attack did not cause concrete peeling. However, the amount of sulfate solution entering the concrete during this period had been increasing. As a result, the mass of the specimens continued to increase. For  $D_1$  and  $D_2$  specimens, many cracks exist in the concrete due to the initial damage. It is easier for external sulfate solution to penetrate the crack interior along the crack tip, and the amount of transmission is large. Besides, the initial damage crack tip is relatively thin. When the expansibility product accumulates and expands, stress concentration is more likely to occur. This leads to the expansion of existing cracks or the formation of new cracks at the tip, thus accelerating the rate of sulfate attack.

### 3.3 Relative Dynamic Modulus of Elasticity

Figure 5 offers a relative dynamic modulus of elasticity (RDME) of concrete specimens with different damage degrees after sulfate attack. It could be found that the RDME of concrete specimens shows the trend of increasing first and then decreasing, which is similar to the research results of Tan et al. (2017). For  $D_0$  specimens without initial damage, the RDME increases continuously before 90 cycles. After 90 cycles, the RDME gradually decreases. However, for  $D_1$  and  $D_2$  specimens, after 30 cycles, the RDME began to decrease. Besides, the change rate of RDME is different with different degrees of damage. Before 30 cycles, the RDME of  $D_2$  specimen

with the largest degree of damage increases the fastest, followed by  $D_1$  and  $D_0$ . At 30 cycles, the RDME of  $D_0$ ,  $D_1$ , and  $D_2$  is 1.027, 1.071, and 1.085, respectively. When the RDME turns to the descending stage, the same  $D_2$  specimen decreases the fastest and  $D_0$  the slowest. At 150 cycles, the RDME of  $D_0$ ,  $D_1$ , and  $D_2$  is 0.952, 0.857, and 0.791, respectively. This indicates that the existence of initial damage of concrete specimens accelerates the degradation rate of sulfate attack on the concrete specimen.

Relative dynamic elastic modulus was measured by ultrasonic wave velocity, which is closely related to the compactness of the specimen. At the early stage of sulfate attack, the sulfate solution permeated into the concrete and interacted with cement hydration products to form expansive products. Those ettringite and gypsum filled the pores and cracks, which resulted in the compacting of the concrete. The ultrasonic wave velocity in the specimen gradually increased and well as the RDME. At the later stage of sulfate attack, the continuous accumulation and expansion of the products led to the development of cracks inside the specimens, leading to loose structure (Gospodinov 2005). The velocity of ultrasonic wave propagation in the specimen gradually decreased as well as the RDME. Under the sulfate wetting–drying cycle, the initial damage degree of specimens significantly affects the process of sulfate attack on concrete. For  $D_0$ , there was no initial damage and the internal structure remains intact. In the process of sulfate attack,

the specimens were broken only relying on the expansion of the product, so the process is relatively slow. Even after 150 days of sulfate attack, the internal damage degree was small, and the relative dynamic elastic modulus remained at 0.952. For  $D_1$  and  $D_2$ , due to the initial damage, there were a large number of internal connectivity cracks. When the specimen was saturated, the sulfate solution filled the interior of the crack. When ettringite is generated inside the cracks, the volume expands, and the stress concentration tends to occur at the tip of the crack. This leads to the rapid development of the cracks along the tip and the rapid destruction of concrete. Therefore, the higher the initial damage degree is, the more penetrating cracks in the interior will be. The expansion force caused by the reaction between cement hydration products and the sulfate ions is more likely to cause new cracks in the specimen. As a result, the internal compactness of the specimen decreases, and the RDME decreases significantly.

## 4 Uniaxial Compression Test

### 4.1 Failure Mode

The uniaxial compression failure mode of concrete with different initial damage is similar. The concrete specimen with initial damage degree  $D_1$  is selected and the uniaxial compression failure process after 150 days of sulfate attack is shown in Fig. 6.



**a** Initial loading stage **b** Mid-loading stage **c** Post-loading stage

**Fig. 6** Failure process of specimen  $D_1$  after 150 sulfate attack cycles.

For the specimen at the initial stage of loading, as shown in Fig. 6a, no obvious crack can be observed on the surface of the specimen. With the increase of loading, many small cracks can be observed at the bottom of the specimen, as can be shown in Fig. 6b. The cracks developed independently, and the surface of the specimen was a little spalling. Gradually, the number of cracks tended to be stable, as shown in Fig. 6c. The width of cracks increased and the specimens were peeled off and crushed.

In the uniaxial compression process of concrete, the phenomena such as skin flaking, internal loose, and local compression can be observed, especially in the areas where sulfate attack deteriorates severely. The observed failure surface shows that the coarse aggregate is intact and few cracks occur. The cracking occurs mainly in the interface between the coarse aggregate and the cement mortar and the interior of the cement mortar, which is consistent with the rule found in reference, indicating that the sulfate attack mainly occurs on the cement paste (Zhang et al. 2013).

The destruction characteristics of concrete specimens with different initial damage under uniaxial compression are shown in Fig. 7.

There are many cracks on the surface of the concrete with different initial damage under uniaxial compression.

These cracks appear at the bottom of the concrete first and then spread upward. One or two cracks are obvious and the width decreases from the bottom to the top of the concrete. The bottom concrete is crushed first. The main crack penetrates the whole specimen when the concrete breaks and the width of the main crack is about 3 mm. With the development of the main crack, one or two secondary cracks appear subsequently. The length of the secondary crack is a little shorter than the main crack and the width is more than 1 mm. It is found that the larger the initial damage of concrete, the larger the width of the crack, the shorter the damage time, and the more serious the damage.

#### 4.1.1 Stress–Strain Curve

To get reliable test results, three specimens were prepared for each variable. Then, three parallel tests were carried out and three curves were obtained for each variable. The deviation between the maximum value and the minimum value was not more than 15%, and the middle curve was used as the experimental result. Therefore, the curve on the figure represents only one specimen.

The stress–strain curves of  $D_0$ ,  $D_1$ , and  $D_2$  specimens after sulfate attack are shown in Figs. 8, 9, 10, respectively. The stress–strain curves of all specimens consist of ascending and descending sections. The initial

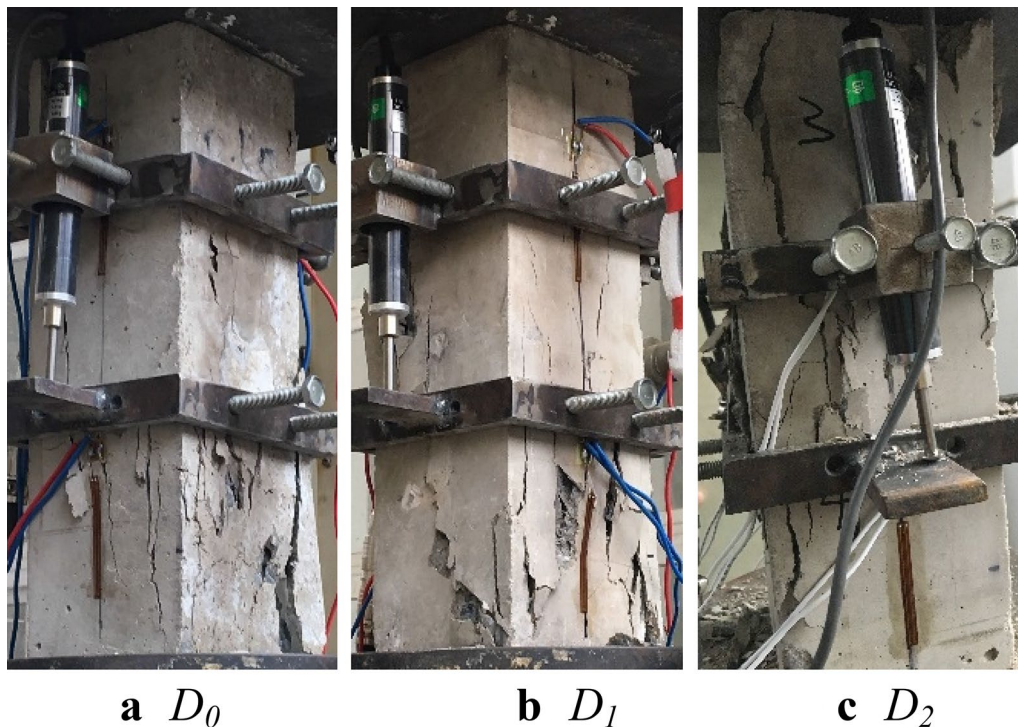


**Fig. 7** Fail mode of specimens with different initial damage under uniaxial compression.

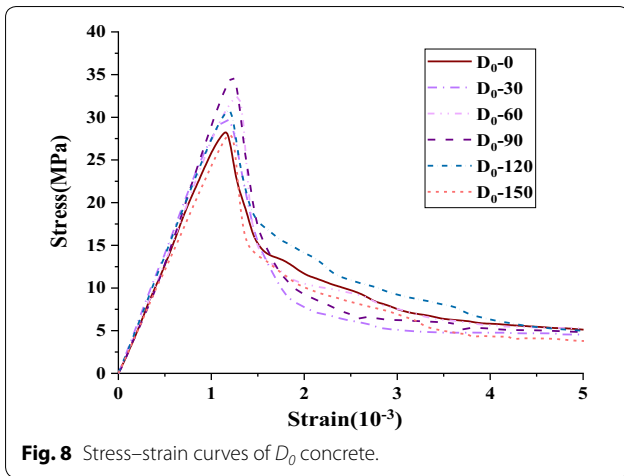


**Fig. 8** Stress–strain curves of  $D_0$  concrete.

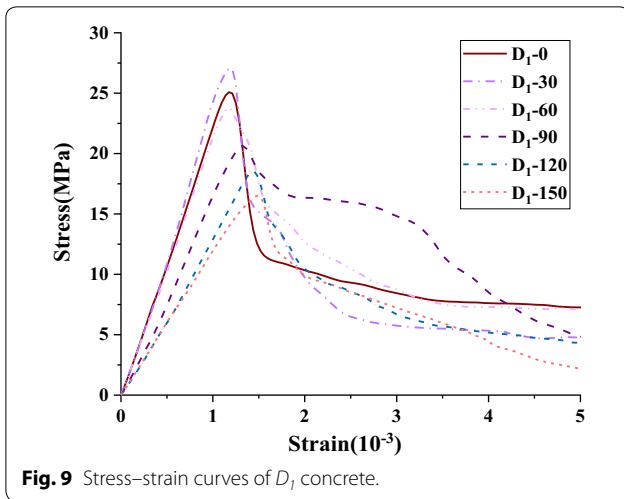


**Fig. 9** Stress–strain curves of  $D_1$  concrete.

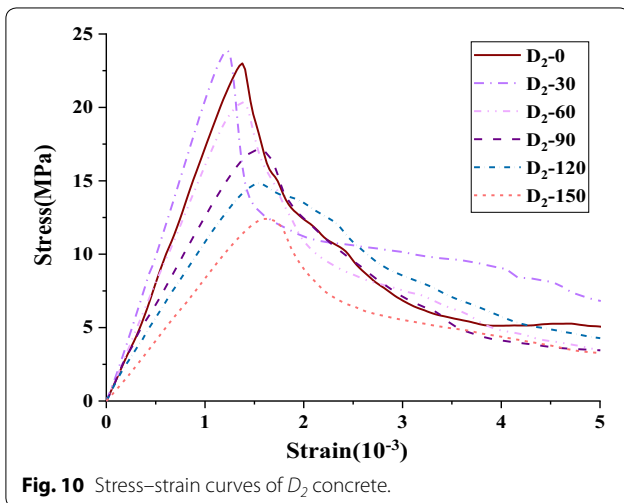


**Fig. 10** Stress–strain curves of  $D_2$  concrete.

**Table 3** Mechanical properties of sulfate attacked specimens.

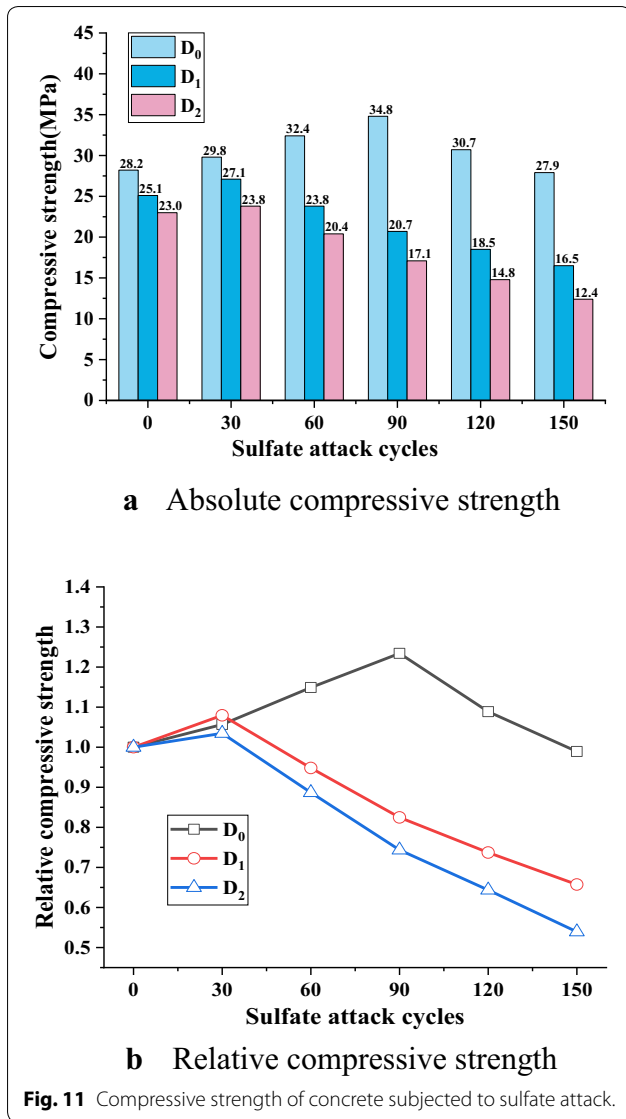
No.	Sulfate attack cycles	$f_{max}$ (MPa)	$E_0$ (GPa)	Peak strain ( $10^{-3}$ )
$D_0$	0	28.2	24.6	1.146
	30	29.8	25.9	1.159
	60	32.4	28.5	1.273
	90	34.8	29.9	1.233
	120	30.7	26.5	1.172
	150	27.9	24.2	1.202
$D_1$	0	25.1	21.9	1.174
	30	27.1	23.5	1.187
	60	23.8	21.3	1.162
	90	20.7	16.5	1.326
	120	18.5	12.9	1.430
	150	16.5	11.9	1.493
$D_2$	0	23.0	17.4	1.378
	30	23.8	20.4	1.225
	60	20.4	16.0	1.384
	90	17.1	12.4	1.560
	120	14.8	10.6	1.556
	150	12.4	8.4	1.641

damage degree has a great influence on the shape of the curves. As can be seen from Fig. 8, for  $D_0$  specimens without initial damage, except for the fluctuation at the highest point of the curve, the stress–strain curve after different sulfate attack cycles was relatively close; this phenomenon is similar to the experimental results of Yang et al. (2019). Compared with  $D_0$ , the stress–strain curves of  $D_1$  and  $D_2$  concrete specimens at different sulfate attack cycles have obvious changes. Before 30 cycles, the peak value of the stress–strain curve gradually increases with the increase of time. However, when the sulfate attack cycles reached 60, the peak value of the curve gradually decreased, and the decline was more obvious when it reached 150 days.

Based on the stress–strain curve, some important physical and mechanical properties such as peak stress ( $f_{max}$ ), peak strain and elastic modulus ( $E_0$ ) can be obtained, which are summarized in Table 3.

**4.1.2 Compressive Strength**

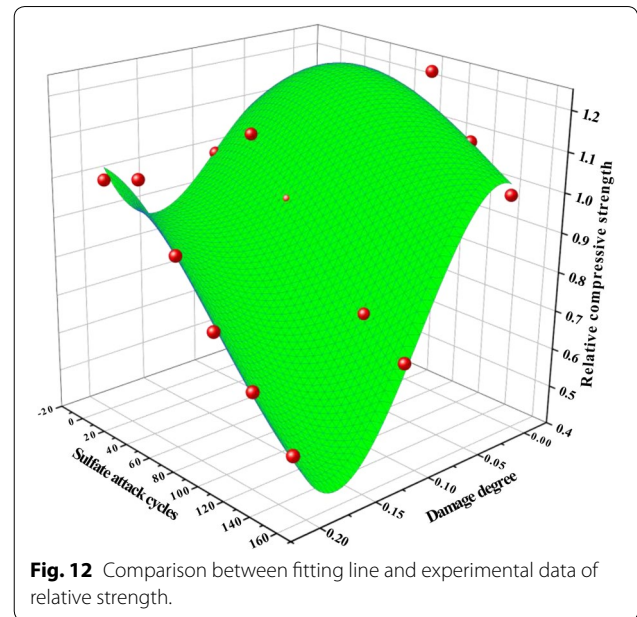
The compressive strength of specimens after different sulfate attack is shown in Table 3 and Fig. 11a. For comparison of data between specimens with different degrees of damage, the relative compressive strength  $R_{fs}$  is calculated by Eq. (4) and shown in Fig. 11b.



$$R_f = \frac{f_{D_j}^i}{f_{D_j}^0} \tag{4}$$

where  $f_{D_j}^i$  is the compressive strength of  $D_0$ ,  $D_1$ , and  $D_2$  specimens after  $i$  sulfate attack cycles.  $f_{D_j}^0$  is the compressive strength of the specimens without sulfate attack.

The compressive strength of concrete specimens with different degrees of damage after the sulfate attack cycle is shown in Fig. 11. It can be seen from the figure that with the increase of sulfate attack cycles, the strength development of specimens shows an increase in the early stage. After a certain sulfate attack cycles, the compressive strength decreases. This phenomenon is similar to the results of Zhou et al. (2016), and this phenomenon is similar to that of relative dynamic modulus of elasticity.



Moreover, the damage degree has an obvious influence on the change of compressive strength. For the  $D_0$  specimen, the strength increased continuously before 90 cycles and decreased after 90 cycles. Before 90 cycles, the expansion product in  $D_0$  fills the internal pores of the concrete, which make the concrete denser and result in improving the physical and mechanical properties. After 90 cycles, the expansion of sulfate corrosion will cause damage to the concrete and reduce the strength. Compared with 90 cycles of  $D_0$ , the compressive strength of  $D_1$  and  $D_2$  specimens with initial damage was reduced to 30 cycles. Besides, with the increase of damage degree, the compressive strength of concrete specimens decreases faster. After 150 cycles, the compressive strength of  $D_0$ ,  $D_1$ , and  $D_2$  and the axial compressive strength is 27.9 MPa, 16.5 MPa, and 12.4 MPa, respectively. The relative compressive strength is 0.989, 0.657, and 0.539, respectively. Therefore, the initial damage degree will significantly accelerate the degradation speed of concrete strength.

Based on the test data in Table 3, the degree of damage and the number of sulfate attack cycles were taken as independent variables and the relative strength as dependent variable. The relationship among them is regressed by Origin software, and the binary function is obtained as Eq. (6).

$$R_f = 0.828 - 0.096 \ln D_j - 0.0002 N_{D_j}^i - 0.0001 (\ln D_j)^2 - 1.89 \times 10^{-5} N_{D_j}^{i2} - 4.66 N_{D_j}^i \ln D_j R^2 = 0.9361 \tag{5}$$

where  $R_f$  is the relative compressive strength,  $D_j$  damage degree of the concrete specimen, and  $N_{D_j}^i$  the number of sulfate attack cycles. The comparison between theoretical values and experimental data is shown in Fig. 12. The coefficient of determination of Eq. (5) is 0.9361, which shows that a good correlation between the equation and the test data.

### 4.1.3 Modulus of Elasticity

According to ASTM C469, the elastic modulus of degraded concrete is calculated by Eq. (6).

$$E = \frac{\sigma_2 - \sigma_1}{\varepsilon_2 - 0.00005} \tag{6}$$

where  $\sigma_2$  is the stress corresponding to 40% of the peak stress.  $\sigma_1$  is the stress corresponding to a strain of 0.00005.  $\varepsilon_2$  is the strain at the stress level  $\sigma_2$ .

The elastic modulus of sulfate attacked concrete was taking the secant modulus at 40% of peak stress from the stress–strain curve. The results of the elastic modulus of specimens after different sulfate attack cycles are shown in Fig. 13a and Table 3. The relative elastic modulus ( $R_E$ ) is calculated by Eq. (7) and shown in Fig. 13b.

$$R_E = \frac{E_{D_j}^i}{E_{D_j}^0} \tag{7}$$

where  $E_{D_j}^i$  is the elastic modulus of  $D_0$ ,  $D_1$ , and  $D_2$  specimens after  $i$  sulfate attack cycles.  $E_{D_j}^0$  is the elastic modulus of  $D_0$ ,  $D_1$ , and  $D_2$  specimens before sulfate attack.

The change of modulus of elasticity of concrete specimens after different cycles of sulfate attack is shown in Fig. 13. Compared with Figs. 12 and 13, the change of elastic modulus is similar to that of compressive strength. In the beginning, the modulus of elasticity increases with the number of sulfate attack. When the number of cycles exceeds a certain value, the elastic modulus begins to decrease with the number of cycles. The critical cycles of  $D_0$  were 90, while  $D_1$  and  $D_2$  were 30. Besides, the damage degree also affects the change rate of elastic modulus. The larger the damage degree is, the greater the change rate is. The curve of the relative elastic modulus of  $D_2$  specimens is steeper than that of  $D_1$  specimens. After 30 sulfate attack cycles, the relative elastic modulus of  $D_1$  and  $D_2$  specimens are 1.07 and 1.17, respectively, and after 150 cycles, the relative elastic modulus of  $D_1$  and  $D_2$  specimens are 0.54 and 0.48, respectively.

Based on the test data in Table 3, the degree of damage and the number of sulfate attack cycles were taken as independent variables and the relative strength as dependent variable. The relationship among them is

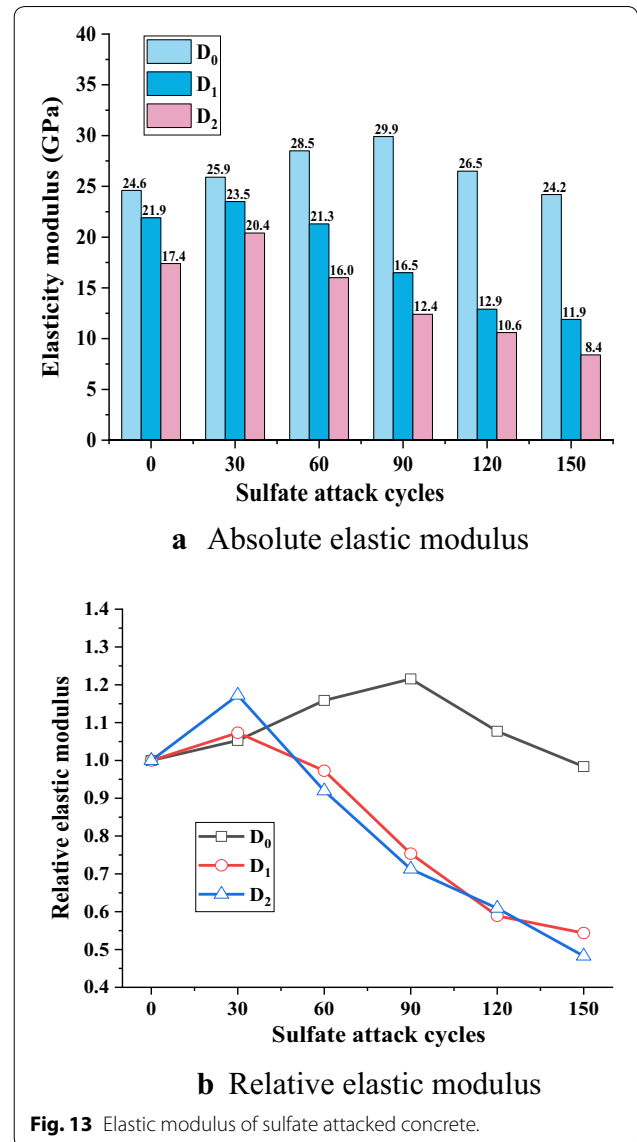
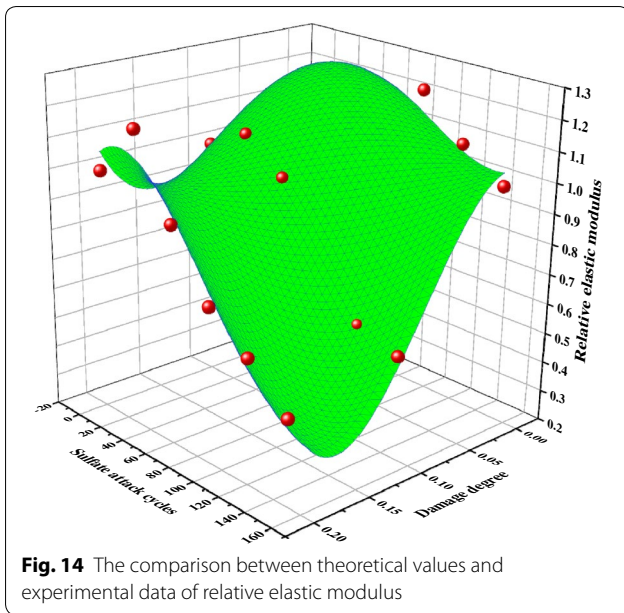


Fig. 13 Elastic modulus of sulfate attacked concrete.

regressed by Origin software, and the binary function is obtained as Eq. (8).

$$R_E = 1.04 - 0.0068 \ln D_j - 0.0005 N_{D_j}^i - 9.89 \times 10^{-6} (\ln D_j)^2 - 2.47 \times 10^{-5} N_{D_j}^{i2} - 5.83 \times 10^{-6} N_{D_j}^i \ln D_j R^2 = 0.9118 \tag{8}$$

where  $R_E$  is the relative compressive strength,  $D_j$  damage degree of the concrete specimen, and  $N_{D_j}^i$  the number of sulfate attack cycles. The comparison between theoretical values and experimental data is shown in Fig. 14. The coefficient of determination of Eq. (8) is 0.9361, which



shows that a good correlation between the equation and the test data.

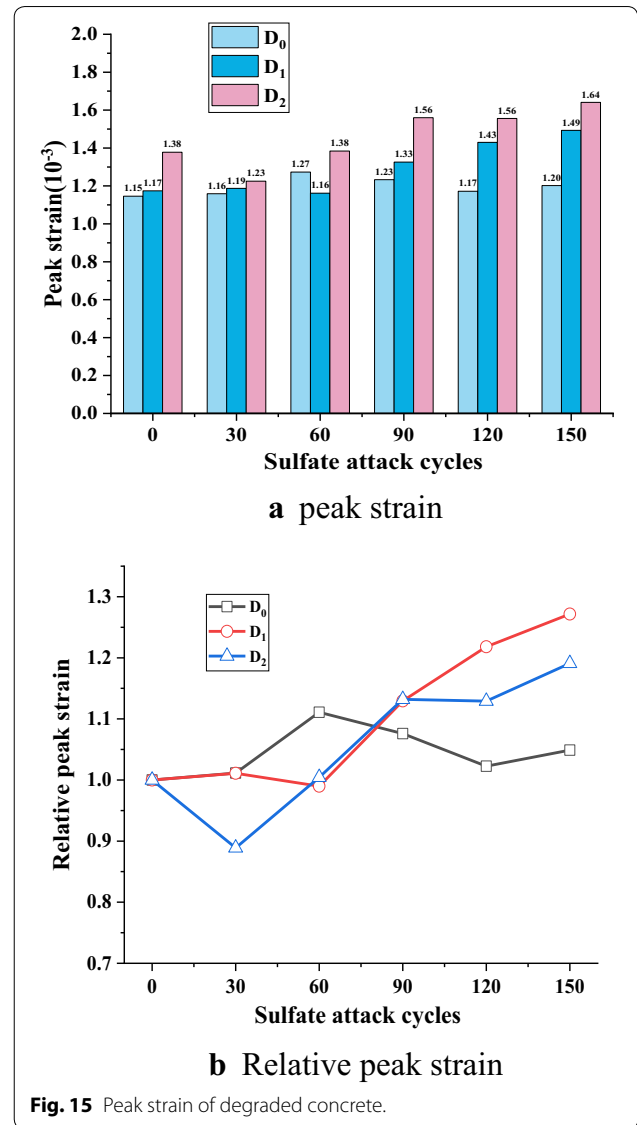
#### 4.1.4 Peak Strain

The results of the peak strain of specimens after different sulfate dry–wet cycles are shown in Fig. 15a and Table 3. The relative peak strain ( $R_s$ ) is calculated by Eq. (9), and shown in Fig. 15b.

$$R_s = \frac{S_{D_j}^i}{S_{D_j}^0} \tag{9}$$

where  $S_{D_j}^i$  is the peak strain of  $D_0$ ,  $D_1$ , and  $D_2$  specimens after  $i$  days of sulfate dry–wet cycles.  $S_{D_j}^0$  is the peak strain of  $D_0$ ,  $D_1$ , and  $D_2$  specimens without sulfate dry–wet cycles.

The peak strain of concrete specimens after different sulfate attack cycles is shown in Fig. 13. It can be seen from the figure that the peak strain of specimens with different initial damage degrees has different rules. For the  $D_0$  specimen, the peak strain did not change obviously under different cycles of sulfate attack, which fluctuates around  $1.2 \times 10^{-3}$ . The relative peak strain also fluctuated around 1.05. From the previous data of compressive strength and modulus of elasticity, it can be found that the mechanical properties of  $D_0$  concrete specimens do not degrade significantly in 150 cycles of sulfate attack. The expansion caused by sulfate corrosion did not cause much damage to the concrete. Therefore, there is no obvious change of deformation ability under the action of pressure. However, the situation of  $D_1$  and  $D_2$  specimens



with initial damage is different from that of  $D_0$ . The peak strain increases with the increase of the sulfate attack cycle. After 150 cycles of sulfate attack, the peak strains of  $D_0$ ,  $D_1$ , and  $D_2$  are 1.2, 1.49, and 1.64, respectively. This is due to the existence of initial damage so that the external sulfate ions can penetrate the concrete quickly. The expansion products are formed rapidly. The expansion product was formed continuously in the cracks, which result in appearing more new cracks. The new crack improves the deformation ability of the concrete specimen, thus increasing the peak strain.

#### 4.1.5 Stress–Strain Model for Sulfate-Attacked Concrete

The stress–strain curve of concrete can reflect the mechanical properties of concrete during compression,

which is necessary for concrete analysis and the establishment of bearing capacity. In this paper, the analytical expression of the stress–strain suggested by Guo and Zhang (2004) was introduced as the basic model equation to predict the stress–strain curves, just as shown in Eqs. (10) and (11).

$$\frac{\sigma}{f'_c} = \frac{A\left(\frac{\varepsilon}{\varepsilon_0}\right) - \left(\frac{\varepsilon}{\varepsilon_0}\right)^2}{1 + (A - 2)\left(\frac{\varepsilon}{\varepsilon_0}\right)} \quad (\varepsilon \leq \varepsilon_0) \quad (10)$$

$$\frac{\sigma}{f'_c} = \frac{1}{B \times \left(\frac{\varepsilon}{\varepsilon_0}\right)^C + 1 - B} \quad (\varepsilon > \varepsilon_0) \quad (11)$$

where  $\sigma$  and  $\varepsilon$  are the actual stress and actual strain value, respectively; and  $\varepsilon_0$  are the peak stress (compressive strength) and peak strain, respectively;  $A$  is a parameter that controls the ascending branch of the curve;  $B$  and  $C$  are parameters that control the descending branch of the curve (Liu et al. 2017).

Equations (10) and (11) can be used to generate the complete stress–strain curve for different  $A$ ,  $B$ , and  $C$  values in a normalized manner. Those values are summarized in Table 4. As the damage degree and sulfate attack cycles increase, the  $A$  values increase gradually.  $A$  value influences the slope of the curve. The value of  $A$  is inversely proportional to the elastic modulus. The larger

the value of  $A$  is, the smaller the elastic modulus is. Just as shown in Table 4, the  $A$  value is ranged from 0.99 to 1.25. The descending part of the stress–strain curve is affected by the  $B$ - and  $C$ -values. However, it is difficult to find out the obvious relationship between  $B$ ,  $C$ , and the damage degree and the sulfate attack cycles from the test results. The comparison of proposed model equations with experimental results is shown in Figs. 16, 17, 18. There is a good correlation between the experimental data with the analytical curves.

#### 4.2 Discussion the Mechanism of Initial Damage on the Degradation of Concrete

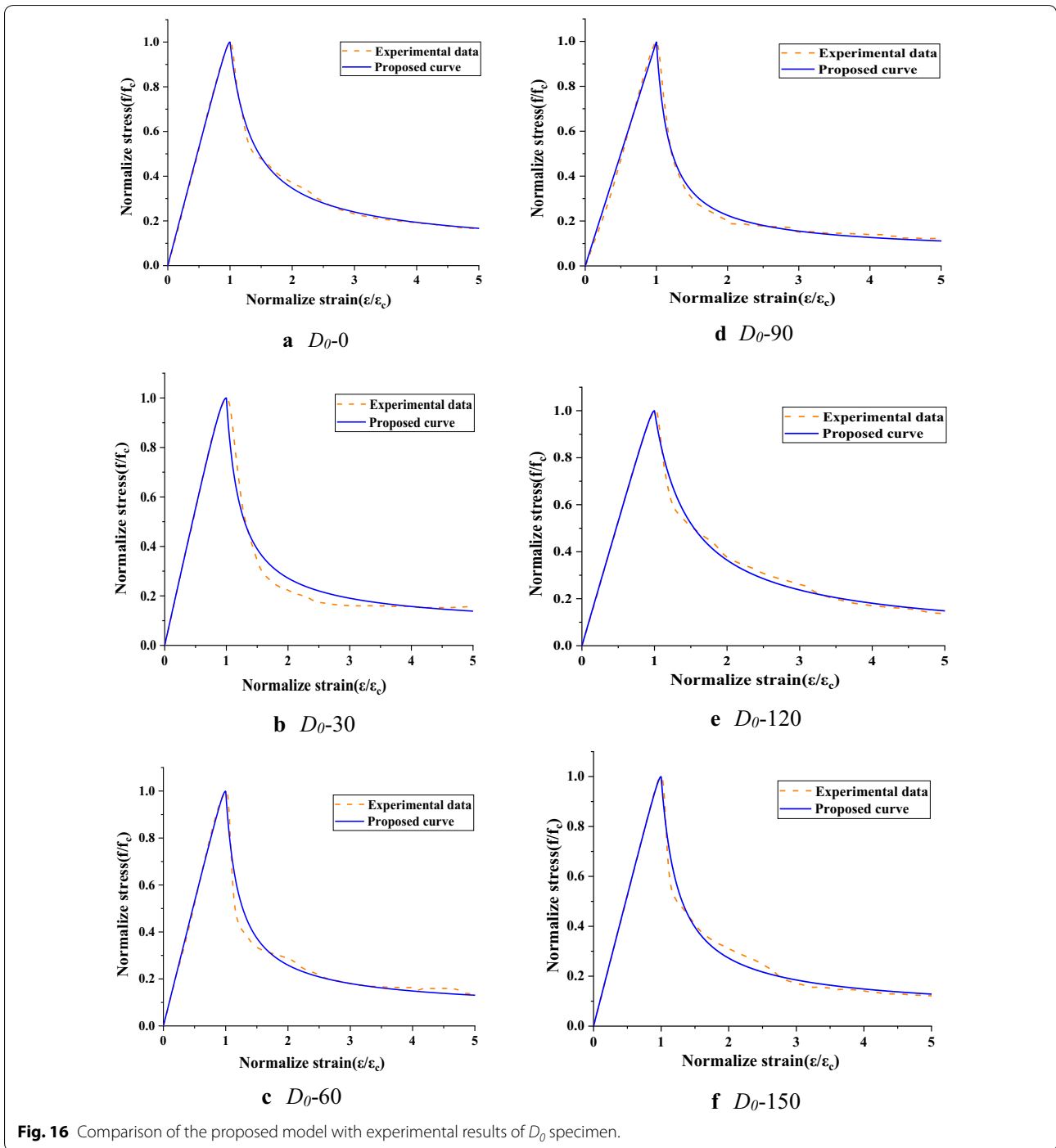
The SEM images of degraded specimens after 30 and 150 sulfate attack cycles are shown in Fig. 19. Energy Dispersive Spectrometer (EDS) shows that the main corrosion product was ettringite. It can be seen from the figure that the initial damage degree has a significant impact on the formation of corrosion products in concrete. For  $D_0$  specimens, ettringite is less visible inside the 30 cycles, and most of them are hydration products CSH gel. However, for  $D_1$  and  $D_2$  samples with initial damage, some of the acicular corrosion products, ettringite, were distributed inside, and the content was significantly higher than that of  $D_0$  samples. When the number of sulfate attack reached 150 cycles, the content of ettringite in  $D_1$  and  $D_2$  samples increased significantly. It can be concluded from the SEM photos that the increase of initial damage degree makes the sulfate ions from outside enter into the concrete quickly. This phenomenon significantly increases the formation of ettringite corrosion products and accelerates the corrosion rate of specimens.

Based on experimental data, the degradation mechanism of concrete with initial damage under the sulfate attack and wetting–drying cycle was discussed, as shown in Figs. 20, 21. The degradation can be divided into three stages. The first stage is the process of sulfate penetrating the concrete. For non-damaged concrete, since there is only some small capillary pore inside of specimen (Fig. 20a), not only the concrete internal sulfate content is low in this stage, but also the sulfate penetration rate is relatively slow. On the other hand, the concrete with initial damage contains large numbers of micro-cracks because of the preloading. As a result, the rate of sulfate penetration is accelerated, and the content of sulfate in concrete also increases (Fig. 20b).

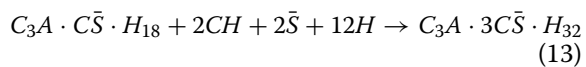
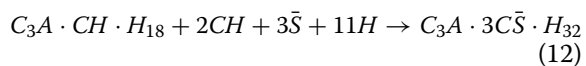
The second stage is the crystallization and expansion stage of the chemical reaction inside the concrete (as shown in Fig. 20c). First, when hydration products contact with sulfate ions, both of its aluminum-containing hydration products become ettringite ( $C_3A \cdot 3\bar{C}\bar{S} \cdot H_{32}$ ), as shown in the following Equations.

**Table 4** Values of parameters  $A$ ,  $B$ , and  $C$  for different specimens.

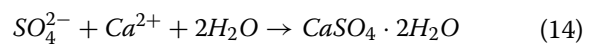
No.	Sulfate attack cycle	Ascending part	Descending part		$R^2$
		$A$	$B$	$C$	
$D_0$	0	1.06079	9.16004	$1.5301 \times 10^{-4}$	0.99614
	30	1.11849	11461.54331	$3.37141 \times 10^{-4}$	0.96945
	60	1.06155	16881.23242	$2.44691 \times 10^{-4}$	0.98164
	90	0.99882	5531.2157	$8.96821 \times 10^{-4}$	0.98984
	120	1.06162	2.92818	0.67443	0.99318
	150	1.05181	18.95907	0.19027	0.98923
$D_1$	0	1.02388	10015.11305	$1.96487 \times 10^{-4}$	0.94518
	30	1.02564	998.55018	0.00344	0.98978
	60	1.02924	1747.3587	$9.09073 \times 10^{-4}$	0.97958
	90	1.03073	0.08231	2.58364	0.97481
	120	0.99689	2.68003	0.67824	0.99554
	150	1.09075	0.68268	1.75409	0.97404
$D_2$	0	1.01727	1870.47901	0.00139	0.97907
	30	1.04629	2365.67288	$7.95432 \times 10^{-4}$	0.93595
	60	1.10379	1.43515	1.12604	0.99511
	90	1.21406	1.45175	1.04073	0.98921
	120	1.19766	0.29678	1.84488	0.99158
	150	1.12493	5.14750	0.36012	0.99323



**Fig. 16** Comparison of the proposed model with experimental results of  $D_0$  specimen.



Second, the gypsum ( $CaSO_4 \cdot 2H_2O$ ) formed by the cation exchange reaction will also cause expansion, as shown in the following Equation.



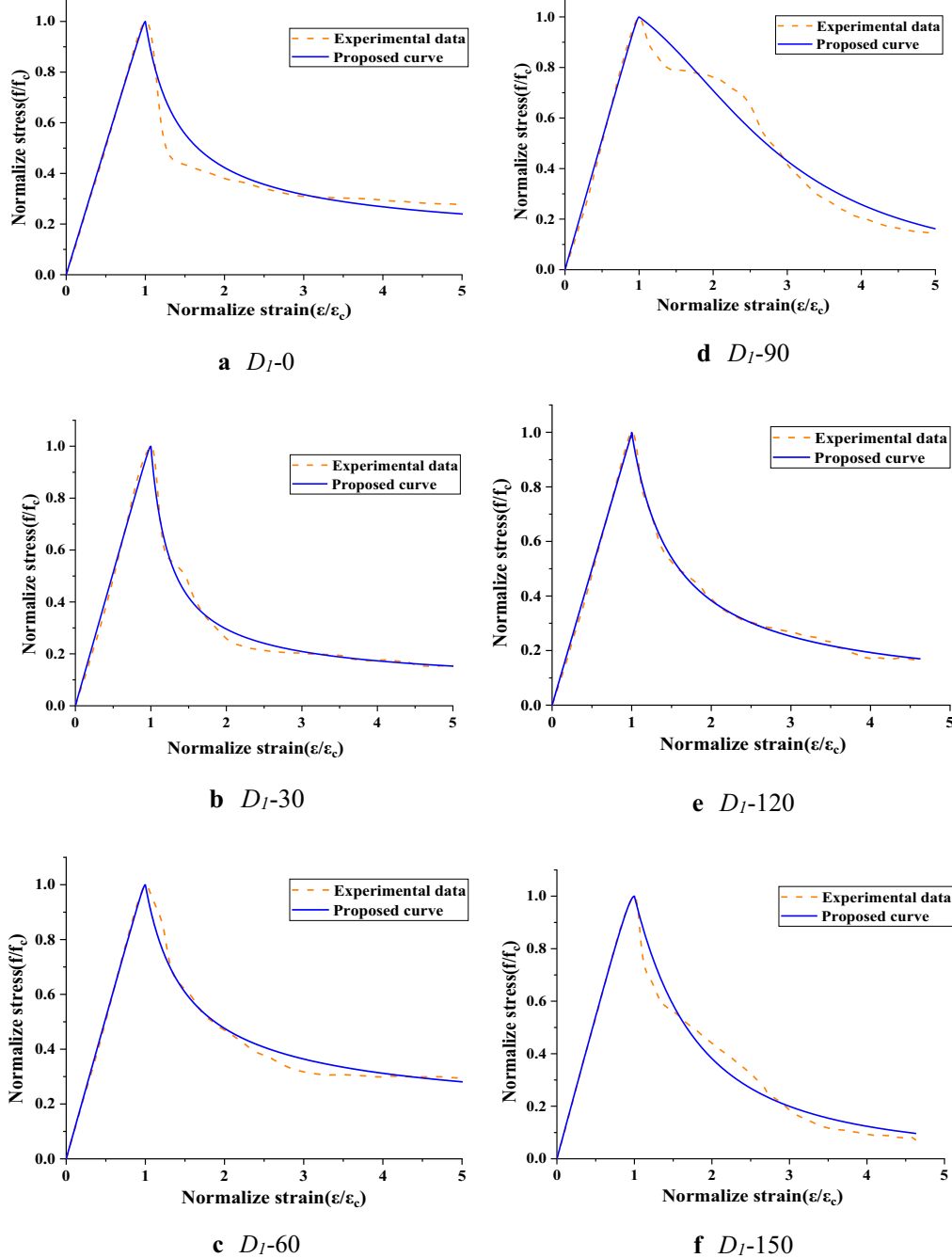


**Fig. 17** Comparison of the proposed model with experimental results of  $D_1$  specimen.

Finally, the occurrence of ettringite and gypsum produces volume expansion. On the one hand, the ettringite and gypsum can squeeze capillary pores and micro-cracks, making cracks gradually expand. The schematic diagram of the effect of sulfate corrosion expansion products on the non-damaged and damaged concrete is shown in Fig. 21. For the concrete with initial damage,

the “extrusion effect” generated by the expansion product is easy to produce stress concentration phenomenon due to its thin micro-crack end, which aggravates the damage degree. With the aggravation of corrosion, these corrosion products accumulate and expand continuously. When the expansion stress is greater than the internal tensile stress, micro-cracks will form and expand, which

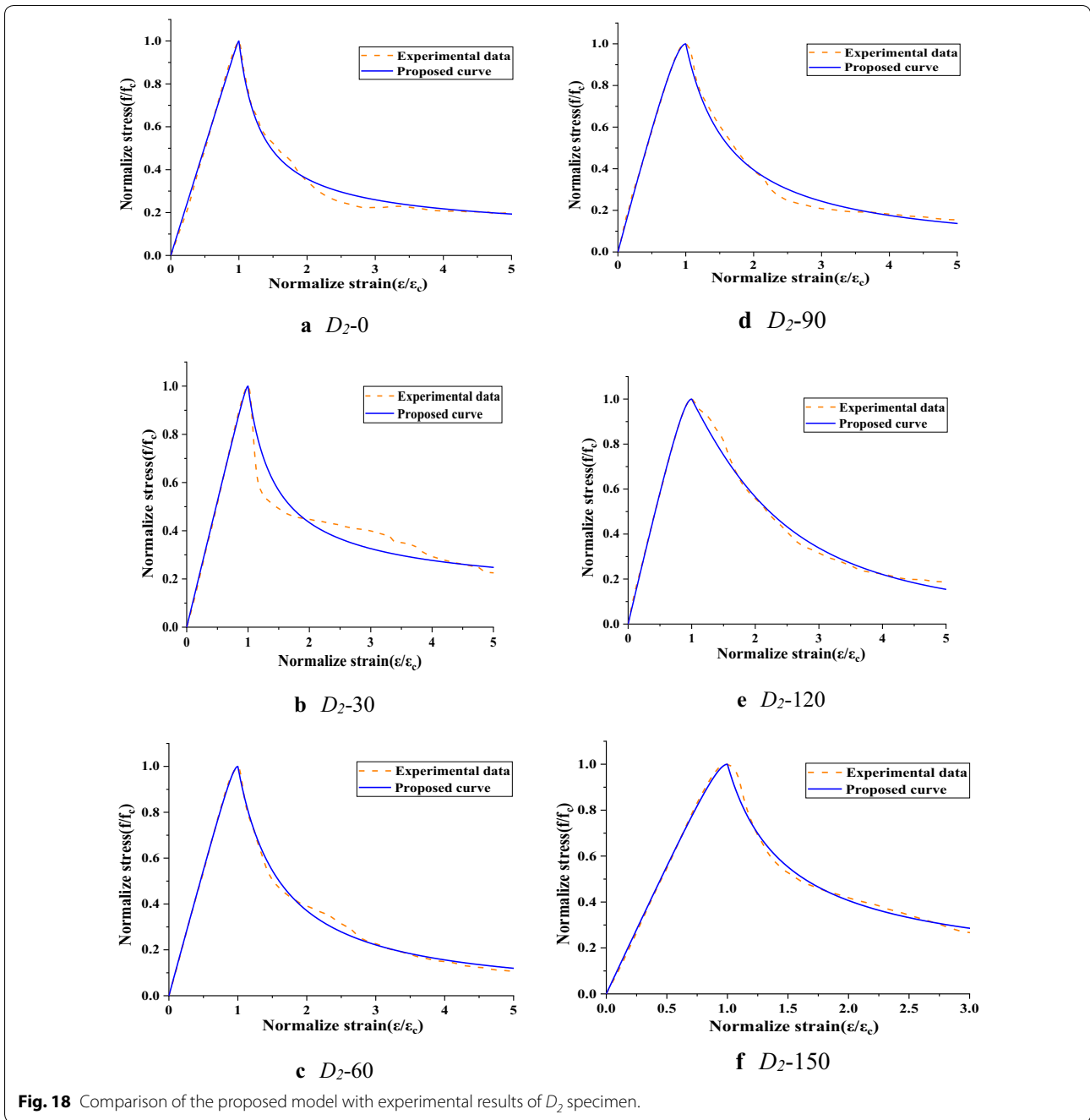


**Fig. 18** Comparison of the proposed model with experimental results of  $D_2$  specimen.

will damage the internal structure of concrete and lead to the decline of macroscopic performance. For non-damaged concrete, although the reaction products will squeeze the wall of capillary pores, the generation and development of cracks are relatively slow because of the difficulty in stress concentration.

Besides, when the specimen in the dry state, the water in the salt solution inside the concrete evaporates quickly, in the salt solution of calcium sulfate solution

mass fraction increases, once reached the supersaturated salt solution in concrete will have salting out, again after absorbing water to form  $CaSO_4 \cdot 2H_2O$ , volume expansion 4–5 times, huge crystallization pressure is formed within the concrete, which can cause expansion cracking of concrete.

Through the combined action of several sulfate corrosion and the dry–wet cycle, the cracks in the concrete gradually widened and increased, and finally came to the

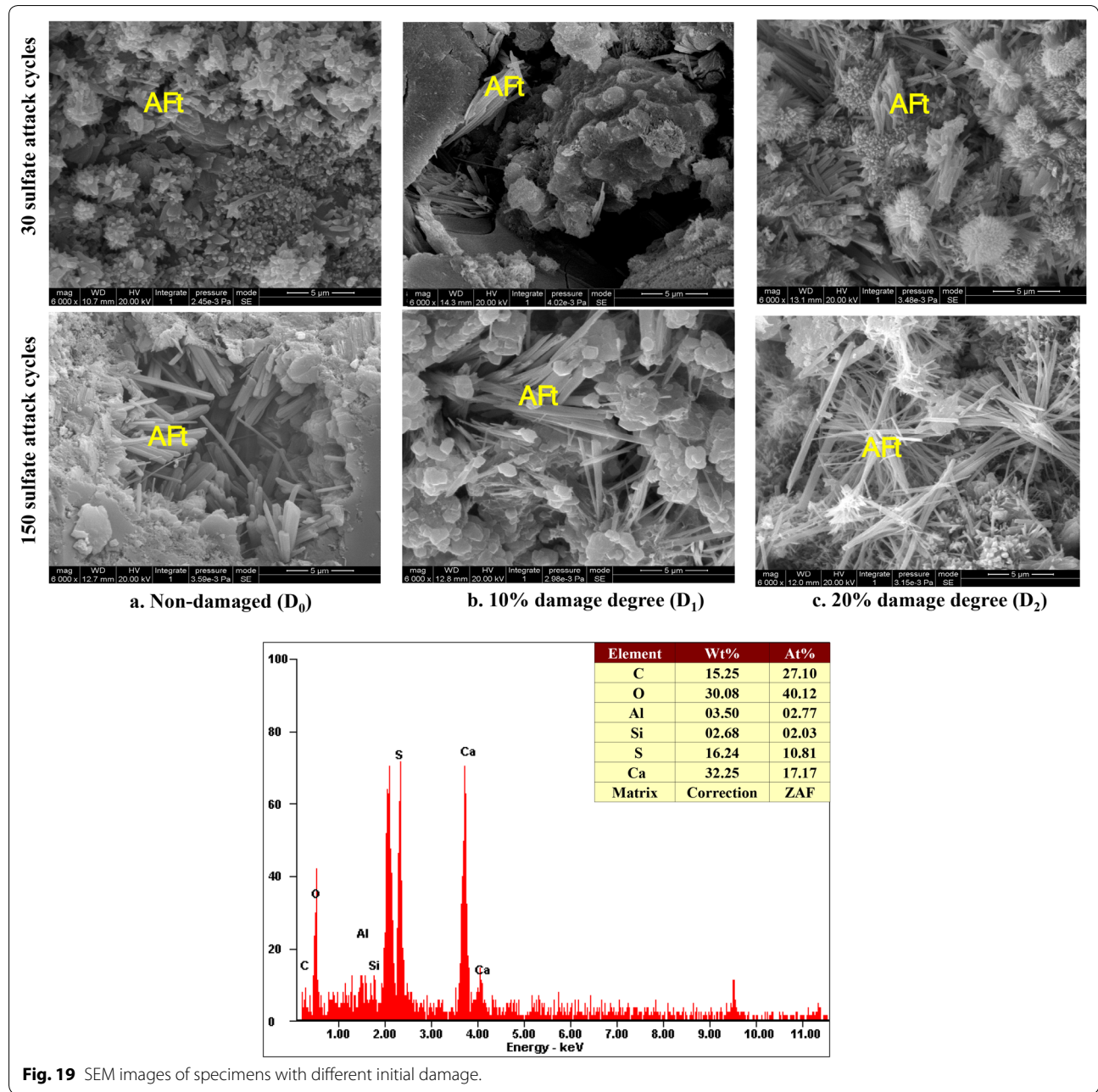
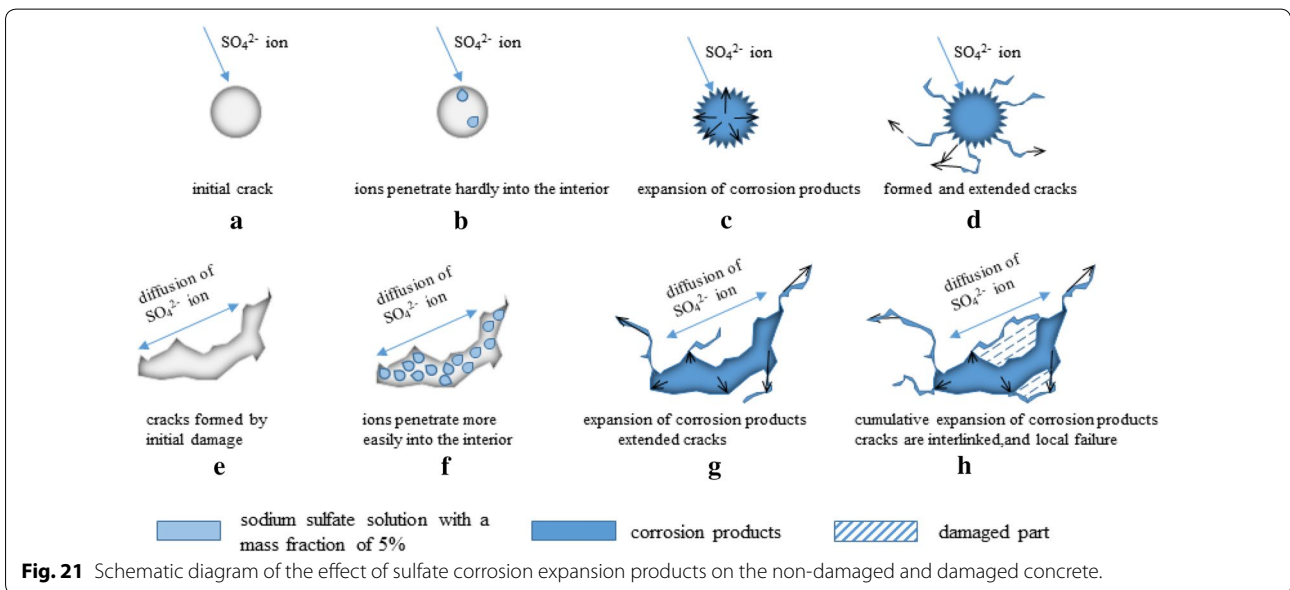
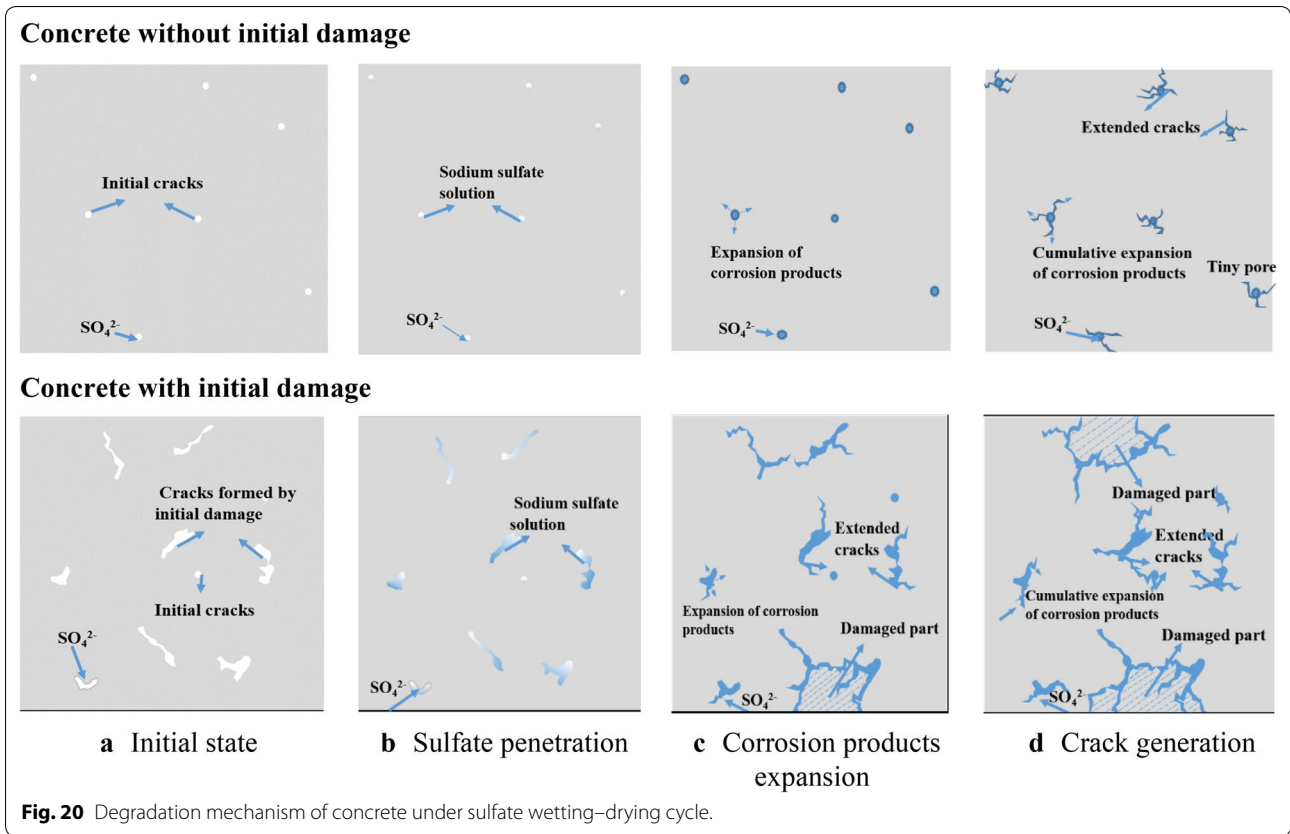


**Fig. 19** SEM images of specimens with different initial damage.

third stage. The surface of the specimen was exfoliated, as shown in Fig. 19d. For non-damaged concrete, because of its slow crack generation, the surface of the specimen spalling less, not obvious. However, for the concrete with initial damage, after several times of sulfate corrosion and dry and wet cycle, the rapid development of micro-cracks leads to local damage and structure loosening, accelerating the process of damage, so the surface of the concrete with more peeling, the phenomenon is obvious. Besides, the specimen had formed large initial damage

before corrosion, resulting in the formation of internal defects such as micro-cracks, and the structure became less dense and more susceptible to sulfate corrosion. Therefore, concrete with initial damage is more prone to damage, and the higher the initial damage, the more serious the damage.



### 5 Conclusions

Three different damage degrees of concrete specimens with non-damaged ( $D_0$ ) and initial damage of 10% ( $D_1$ ) and 20% ( $D_2$ ) were prefabricated. Those concrete

specimens were placed under sulfate attack and drying–wetting cycles for investigating the degradation of concrete. The following conclusions can be drawn.

- (1) The mass of the  $D_0$  specimen had been increasing continuously before 150 sulfate attack cycles. The mass of  $D_1$  and  $D_2$  had been increasing before 60 cycles, and decreasing after 60 cycles. At 150 cycles, the mass loss of  $D_0$ ,  $D_1$  and  $D_2$  was  $-1.054\%$ ,  $0.29\%$  and  $3.20\%$ , respectively.
- (2) Relative dynamic modulus of elasticity of  $D_0$  specimen increases continuously before 90 sulfate attack cycles. After 90 cycles, the RDME gradually decreases. However, for  $D_1$  and  $D_2$  specimens, after 30 cycles, the RDME began to decrease. The existence of initial damage of concrete specimens accelerates the degradation rate of sulfate attack on the concrete specimen.
- (3) The initial damage degree has a great influence on the shape of the stress–strain curves. The stress–strain curve of  $D_0$  after 150 sulfate attack times was relatively similar. For  $D_1$  and  $D_2$  specimens, with the increase of sulfate attack times, the peak value of the curve becomes lower and the ascending section becomes more gentle.
- (4) The damage degree has an obvious influence on the change of compressive strength and elastic modulus. For the  $D_0$  specimen, the compressive strength and elastic modulus increased continuously before 90 cycles and decreased after 90 cycles. The compressive strength and elastic modulus of  $D_1$  and  $D_2$  specimens began to decrease after 30 cycles.
- (5) The peak strain of  $D_0$  did not change obviously under different cycles of sulfate attack, which fluctuates around  $1.2 \times 10^{-3}$ . The relative peak strain also fluctuated around 1.05. However, the peak strain of  $D_1$  and  $D_2$  increases with the increase of the sulfate attack cycle. After 150 cycles of sulfate attack, the peak strain of  $D_0$ ,  $D_1$ , and  $D_2$  are 1.2, 1.49, and 1.64, respectively.
- (6) Based on the analysis of experimental data, the degradation mechanism of concrete with initial damage under the sulfate wetting–drying cycle was discussed.

#### Acknowledgements

Thanks Dr. Su Fan and Dr. Yang Jing of Advanced analysis and testing center of Nanjing Forestry University for the help of the experimental tests.

#### Authors' contributions

YL analyzed and interpreted the experimental data regarding the sulfate attack and compressive tests, and was a major contributor in writing the manuscript. WZ designed the experiment and was the director of scientific research funds. FW and HL are the executors of the compressive test. YZ and GX analyzed experimental data regarding compressive tests and set up the stress–strain model. All authors read and approved the final manuscript.

#### Authors' information

Yujing Lv, Mater student, School of Civil Engineering, Nanjing Forestry University, Nanjing, 210037, China, lvyujing1994@163.com.

Wenhua Zhang, Associate Professor, School of Civil Engineering, Nanjing Forestry University, Nanjing, 210037, China, zhangwenhua2009@163.com.

Fan Wu, Mater Student, School of Civil Engineering, Nanjing Forestry University, Nanjing, 210037, China, wufan970503@163.com.

Huang Li, Mater student, School of Civil Engineering, Nanjing Forestry University, Nanjing, 210037, China, huangli0302@163.com.

Yunsheng Zhang, Professor, School of Materials Science and Engineering, Southeast University, Nanjing, 211189, China, zhangys279@163.com.

Guodong Xu, Senior Engineer, Jiangsu Testing Center for Quality of Construction Engineering, Nanjing, 210028, China.

#### Funding

This research was financially supported by the National Natural Science Foundation of China (51678309, 51978339), State Key Laboratory of Silicate Materials for Architectures (SYSJJ2017-09) (Wuhan University of Technology), Priority Academic Program Development Jiangsu Higher Education Institutions (PDPA).

#### Availability of data and materials

Not applicable.

#### Competing interests

The authors declare that they have no competing interests.

#### Author details

<sup>1</sup> School of Civil Engineering, Nanjing Forestry University, Nanjing 210037, China. <sup>2</sup> School of Materials Science and Engineering, Southeast University, Nanjing 211189, China. <sup>3</sup> Jiangsu Testing Center for Quality of Construction Engineering, Nanjing 210028, China.

Received: 26 February 2020 Accepted: 15 June 2020

Published online: 03 August 2020

#### References

- Aye, T., & Oguchi, C. T. (2011). Resistance of plain and blended cement mortars exposed to severe sulfate attacks. *Construction and Building Materials*, *25*(6), 2988–2996.
- Bonakdar, A., Mobasher, B., & Chawla, N. (2012). Diffusivity and micro-hardness of blended cement materials exposed to external sulfate attack. *Cement & Concrete Composites*, *34*(1), 76–85.
- Chen, F., Gao, J., et al. (2017). Degradation progress of concrete subject to combined sulfate–chloride attack under drying–wetting cycles and flexural loading. *Construction and Building Materials*, *151*, 164–171.
- Chen, J., Qian, C., & Song, H. (2016). A new chemo-mechanical model of damage in concrete under sulfate attack. *Construction and Building Materials*, *115*, 536–543.
- Feng, P., Garboczi, E. J., Miao, C., et al. (2015). Microstructural origins of cement paste degradation by external sulfate attack. *Construction and Building Materials*, *96*, 391–403.
- Gao, J., Yu, Z., Song, L., et al. (2013). Durability of concrete exposed to sulfate attack under flexural loading and drying–wetting cycles. *Construction and Building Materials*, *39*, 33–38.
- GB (2009) GB/T 50082-2009: Standard for test methods of long-term performance and durability of ordinary concrete, Ministry of Construction of the People's Republic of China, Beijing, China. (in Chinese).
- Gospodinov, P. N. (2005). Numerical simulation of 3D sulfate ion diffusion and liquid push out of the material capillaries in cement composites. *Cement and Concrete Research*, *35*(3), 520–526.
- Guo, Z., Zhang X. (2004) Experimental study on stress–strain complete curve of concrete under monotonic loading. Industrial Construction.
- Helson, O., Eslami, J., Beaucour, A. L., Noumowe, A., & Gotteland, P. (2018). Durability of soil mix material subjected to wetting/drying cycles and external sulfate attacks. *Construction and Building Materials*, *192*, 416–428.

- Hu, J., & Wu, J. (2019). Mechanical properties and uni-axial compression stress–strain relation of recycled coarse aggregate concrete subjected to salt-frost cycles. *Construction and Building Materials*, 197, 652–666.
- Hussein, L., Amleh, L., Siad, H., et al. (2018). Effect of very severe sulfate environment on bonded composite concrete system. *Construction and Building Materials*, 191, 752–763.
- Irdart, A. E., López, C. M., & Carol, I. (2011). Chemo-mechanical analysis of concrete cracking and degradation due to external sulfate attack: a meso-scale model. *Cement & Concrete Composites*, 33(3), 411–423.
- Irassar, E. F., Bonavetti, V. L., & González, M. (2003). Microstructural study of sulfate attack on ordinary and limestone Portland cements at ambient temperature. *Cement and Concrete Research*, 33(1), 31–41.
- Jiang, L., & Niu, D. (2016). Study of deterioration of concrete exposed to different types of sulfate solutions under drying-wetting cycles. *Construction and Building Materials*, 117, 88–98.
- Liu, Z., Chen, W., Wenhua, Z., et al. (2017). Complete stress-strain behavior of ecological ultra-high-performance cementitious composite under uniaxial compression. *ACI Materials Journal*, 114(5), 783–794.
- Liu, F., You, Z., et al. (2020). External sulfate attack on concrete under combined effects of flexural fatigue loading and drying-wetting cycles. *Construction and Building Materials*, 249, 118224.
- Niu, D., Wang, Y., et al. (2015). Experiment study on the failure mechanism of dry-mix shotcrete under the combined actions of sulfate attack and drying–wetting cycles. *Construction and Building Materials*, 81, 74–80.
- Rozière, E., Loukili, A., El Hachem, R., et al. (2009). Durability of concrete exposed to leaching and external sulphate attacks. *Cement and Concrete Research*, 39(12), 1188–1198.
- Siad, H., Kamali-Bernard, S., Mesbah, H. A., et al. (2013). Characterization of the degradation of self-compacting concretes in sodium sulfate environment: influence of different mineral admixtures. *Construction and Building Materials*, 47, 1188–1200.
- Sun, C., Chen, J., Zhu, J., et al. (2013). A new diffusion model of sulfate ions in concrete. *Construction and Building Materials*, 39, 39–45.
- Sun, J., et al. (2018). Influences of limestone powder on the resistance of concretes to the chloride ion penetration and sulfate attack. *Powder Technology*, 338, 725–733.
- Tan, Y., Yu, H., Ma, H., et al. (2017). Study on the micro-crack evolution of concrete subjected to stress corrosion and magnesium sulfate. *Construction and Building Materials*, 141, 453–460.
- Thaulow, N., & Sahu, S. (2004). Mechanism of concrete deterioration due to salt crystallization. *Materials Characterization*, 53(2–4), 123–127.
- Wang, Y., Cao, Y., et al. (2019). Water absorption and chloride diffusivity of concrete under the coupling effect of uniaxial compressive load and freeze–thaw cycles. *Construction and Building Materials*, 209, 566–576.
- Yang, D., Yan, C., Liu, S., et al. (2019). Stress–strain constitutive model of concrete corroded by saline soil under uniaxial compression. *Construction and Building Materials*, 213, 665–674.
- Zhang, M., Chen, J., Lv, Y., et al. (2013). Study on the expansion of concrete under attack of sulfate and sulfate–chloride ions. *Construction and Building Materials*, 39, 26–32.
- Zhou, Y., Li, M., Sui, L., et al. (2016). Effect of sulfate attack on the stress–strain relationship of FRP-confined concrete. *Construction and Building Materials*, 110, 235–250.
- Zhou, C., Zhu, Z., Wang, Z., et al. (2018). Deterioration of concrete fracture toughness and elastic modulus under simulated acid–sulfate environment. *Construction and Building Materials*, 176, 490–499.
- Zuo, X. B., & SUN, W. (2009). Full process analysis of damage and failure of concrete subjected to external sulfate attack. *Journal of The Chinese Ceramic Society*, 37(7), 1063–1067.

#### Publisher's Note

Springer Nature remains neutral with regard to jurisdictional claims in published maps and institutional affiliations.

Submit your manuscript to a SpringerOpen® journal and benefit from:

- Convenient online submission
- Rigorous peer review
- Open access: articles freely available online
- High visibility within the field
- Retaining the copyright to your article

---

Submit your next manuscript at ► [springeropen.com](https://www.springeropen.com)

---